



**Sulfur Resilient Nickel based Catalysts for Steam Reforming
of Jet Fuel**

| | |
|-------------------------------|---|
| Journal: | <i>Catalysis Science & Technology</i> |
| Manuscript ID | CY-ART-08-2020-001559.R1 |
| Article Type: | Paper |
| Date Submitted by the Author: | 15-Oct-2020 |
| Complete List of Authors: | Brady, Casper; University of Delaware, Chemical Engineering Pan, Jian; University of Delaware, Chemical Engineering Xu, Bingjun; University of Delaware, Chemical Engineering |
| | |

ARTICLE

Sulfur Resilient Nickel based Catalysts for Steam Reforming of Jet Fuel

Casper Brady, Jian Pan, and Bingjun Xu*

Received 00th January 20xx,
Accepted 00th January 20xx

DOI: 10.1039/x0xx00000x

Sulfur resilient steam reforming catalysts are of great interest for the development of solid oxide fuel cell systems for aeronautic applications. We demonstrate that nickel-manganese catalysts exhibit substantially improved stability during steam reforming of sulfur containing fuels via a sulfur spillover strategy as compared to monometallic nickel catalysts. This is established via detailed deactivation studies of catalysts in steam reforming conditions with sulfur containing model fuels and real jet fuels (JP-8). Through detailed characterization of spent catalysts, we establish that the increased sulfur resilience is imparted by an increased sulfur capacity due to scavenging by manganese oxide species in close proximity to active nickel particles. Results presented in this work could pave the way for practical application of precious-metal-free steam reforming catalysts in sulfur rich streams, both in aeronautic SOFC systems and other applications.

Introduction

There has been growing interest in applying solid oxide fuel cells (SOFCs) to use in the aviation industry as auxiliary power units¹⁻⁵. While several proposed SOFC-based systems have the potential to dramatically increase the efficiency of auxiliary power units on airplanes, the extreme temperatures (800 - 1000 °C) required for high oxygen ion conductivity in traditional oxide conducting electrolytes⁶ have limited their practical application. In the last decade, the advent of proton conducting solid oxide fuel cells^{7,8} has enabled the production of SOFCs with high performance at temperatures as low as 400-500 °C. Meanwhile, the utilization of proton conducting electrolytes does impose additional technical barriers, the primary being that proton conducting fuel cells cannot be directly powered by hydrocarbons without cofeeding steam. In order to utilize jet fuels in proton conducting SOFCs, steam reforming, either external or internal to the fuel cell stack, must be used to produce hydrogen, which can subsequently be used as fuel in the cell. Jet fuels are subject to far less stringent sulfur content restrictions than other fuels, with certain samples of military (JP-8) and commercial fuels (Jet A) containing sulfur concentrations up to 3000 ppm⁹. The vast majority of metals that are catalytically active for steam reforming are susceptible to sulfur poisoning¹⁰⁻¹³. Thus, lower temperature operation and the inclusion of a steam reforming catalyst incur a significant technical challenge: any on-board steam reforming catalyst must be reasonably stable in sulfur containing streams. Thus, it is imperative to develop sulfur-resistant steam reforming catalysts for the wide adoption of SOFCs in the aerospace industry.

As steam reforming typically is conducted at elevated temperatures, simple thermodynamic considerations can offer substantial guidance on catalyst design. It is well established that under steam reforming conditions H₂S, the most thermodynamic favorable gas phase sulfur species, is readily formed from introduced organosulfur compounds^{14,15}. Sulfur deactivation of catalyst surfaces is usually the result of the formation of monolayers or submonolayers of surface metal sulfides, which passivate the metal particle and suppress activity¹⁰⁻¹³. For most common catalytic metals, the thermodynamics of sulfide monolayers have been probed experimentally^{10-13, 16}. Extensive theoretical work also exists for the determination of these values via first principles calculations^{17, 18}. It is generally accepted that the stability of these films trends roughly with the stability of the least sulfided stable bulk phase of the metal,¹³ i.e., the metal sulfide phase with the lowest S:Metal ratio which has been shown to form a stable bulk phase. Figure S1 shows a collection of heats of adsorption of various sulfur monolayers including both experimentally^{10-13, 16} and computationally determined values¹⁸ plotted against experimentally determined heats of formation for the least sulfided stable metal sulfide phase of the corresponding metal¹⁹⁻²⁴. A general linear correlation between the thermochemical properties of 2-dimensional and 3-dimensional metal sulfides allows for convenient assessment of the relative stability of monolayers of metal sulfides for differing metals based only on readily available thermochemical data (ΔH_f° of bulk sulfides). This correlation between monolayer stability and bulk sulfide stability enables a simple design strategy for sulfur resilient multi-component catalysts in which one metal acts primarily as a catalyst and another acts primarily as a selective sulfur adsorbent; with the second element selected based on the enthalpy of formation of its bulk sulfide. As long as the two components are in close enough proximity for spillover of sulfur to occur and do not form a new phase, initially bound sulfur should preferentially bind to the sacrificial particles, sparing the catalytically active material from sulfur deactivation until saturation of the sacrificial particles. This strategy has been shown to be effective for Ni-Rh catalysts²⁵⁻²⁷, in which supported Rh particles are proposed to act as the majority steam reforming catalyst and Ni particles serve as a sacrificial surface

Center for Catalytic Science and Technology, Department of Chemical and Biomolecular Engineering, University of Delaware, 150 Academy Street, Newark, Delaware

(ESI) available: Additional experimental data is included in the supplementary information. See DOI: 10.1039/x0xx00000x

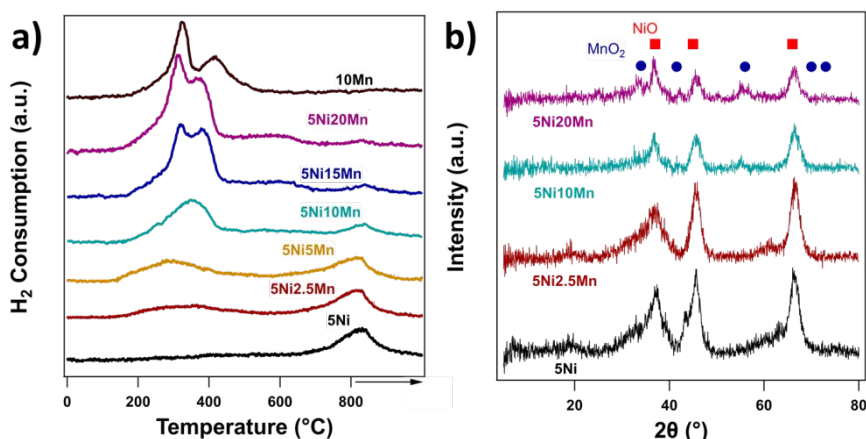


Figure 1: Characterization of pre-catalyst materials a) TPR profiles of monometallic and multi-component catalysts b) Powder XRD patterns of selected calcined catalysts.

for sulfur deactivation. While this multi-component catalyst is dramatically more stable than a monometallic rhodium catalyst with the same loading, rhodium is 3-4 orders of magnitude more expensive than nickel on a mass basis²⁸. Thus, if the size of catalyst bed is not a limiting factor, a much larger bed of a monometallic nickel catalyst would yield the same stability as this multi-component catalyst for a substantially lower cost. In order to design a multi-component catalyst that exhibits enhanced stability without increasing cost we apply this sulfur spillover strategy to multi-component nickel-based catalysts without the use of precious metals. To achieve this, we utilize multi-component catalysts with a relatively inexpensive metal active for steam reforming (nickel) and a secondary inexpensive material to act as a sulfur scavenger. Based on the simple relation between the heats of adsorption of sulfides onto metal surfaces and the heats of formation of the respective bulk sulfides we select manganese as a potential sacrificial sulfur adsorbent owing to the high formation enthalpy of MnS ($\Delta H_f^\circ = -278$ kJ/mol S)²⁹, as compared to that of Ni ($\Delta H_f^\circ = -172$ kJ/mol S). It is important to note that manganese is not expected to be in the metallic state in the steam reforming environment (reduction of manganese oxides to metallic manganese by H₂ requires extreme temperatures¹⁹). This simple thermodynamic analysis does not take the removal of surface lattice oxygen into account, which would be necessary to form a monolayer or sub-monolayer of MnS sulfide on a MnO particle. Meanwhile, MnO is also prone to exhibit a certain degree of oxygen non-stoichiometry³⁰ and manganese oxides have been shown to be effective sulfur adsorbents in streams with high H₂S concentration.³¹⁻³³ Thus, Ni-MnO_x based steam reforming catalysts are investigated to leverage the potential sulfur spillover from metallic Ni to MnO for enhanced sulfur resilience. While existing literature has evaluated Ni-MnO_x based catalysts for steam reforming³⁴⁻³⁷, to our knowledge no systematic investigation has been conducted to evaluate the impact of MnO_x on the sulfur resilience of Ni based reforming catalysts. In addition, this work also extends the S spillover strategy to more affordable elements such as Mn. MnO_x has also seen significant use as a promoter in Fischer-Tropsch catalysts³⁸⁻⁴⁰ in which MnO_x acts to increase selectivities toward long chain linear alcohols and olefins.

Results and Discussion

Catalyst Preparation and Characterization

A series of monometallic and multi-component catalysts containing both nickel and/or manganese have been synthesized and characterized (Table 1 and Figure S2). All catalysts are synthesized via standard wetness impregnation with Ni (II) nitrate and Mn (II) nitrate as metal precursors and dispersible boehmite as a support precursor. Upon calcination at 500 °C, boehmite typically forms γ -Al₂O₃⁴¹, such that our synthesis should yield Ni-MnO_x catalysts supported on γ -Al₂O₃. Synthesized samples are characterized via X-ray fluorescence (XRF) spectroscopy, powder X-ray diffraction (XRD), temperature programmed reduction (TPR), and CO chemisorption. For ease of discussion each catalyst is referred to by a simple designation given in Table 1, in which the number before the metal element refers to its weight percentage. NiB and NiMnB refer to unsupported Ni and NiMn, respectively. The measured Mn:Ni molar ratios by XRF generally agree with the nominal values. Ni dispersions on supported multi-component catalysts determined by CO chemisorption after reduction at 800 °C show that it is not sensitive to the Mn loading at a constant Ni loading (3.3-3.7%, Table 1). In order to understand the state of the nickel and manganese in the synthesized catalysts, they are characterized by temperature programmed reduction (TPR, Figure 1a). 5Ni exhibits a single reduction peak centered at 790 °C. While this is significantly higher than is typically expected for bulk nickel samples, it is expected of low weight loadings of nickel supported on alumina, as the majority of nickel is in the form of NiAlO₄, which is more difficult to reduce^{42, 43}. With the addition of small amounts of manganese (5Ni5Mn, 5Ni10Mn) a broad reduction peak is observed at 200-500 °C. While this peak corresponds to the same reduction temperature as monometallic manganese catalysts, its shape is different. During calcination in air at 500 °C, Mn supported on Al₂O₃ typically forms MnO₂ which reduces in two phases (MnO₂ → Mn₃O₄ followed by Mn₃O₄ → MnO)⁴⁴ in the TPR, causing two distinct, but overlapping reduction peaks, as in the TPR trace corresponding to 10Mn. In the 10Mn sample reduction peaks centered at ~320 °C and 420 °C, with FWHM of ~60 °C and ~100 °C respectively, are observed, while a single broad peak is observed for our 5Ni5Mn sample (centered at ~310 °C with a FWHM of 210 °C). This single broad peak, indicates that the manganese oxide particles formed during calcination in multi-component catalysts are either very small or amorphous; possessing the same general reducibility of

MnO₂ but reducing to MnO in a less stepwise manner. The nickel reduction peak also shifts substantially to lower temperatures and reduces in intensities at higher manganese loadings (Figure 1a). While the high temperature nickel reduction peak attributable to the reduction of NiAlO₄ is always present to a certain degree, nickel reduction in samples with high manganese loadings (5Ni15Mn, 5Ni20Mn) seems to occur in a broad temperature range between 400 and 600 °C, similar to nickel reduction in high weight loading Ni-Al₂O₃ catalysts (Ni wt% > 10%) but substantially higher than that of bulk nickel (200 - 250 °C).³⁵ This could be attributed to the oxygen transfer between nickel and manganese phases during reduction as a result of close association among particles. Another possibility is that manganese addition prevents the formation of NiAlO₄ during calcination by preferentially forming MnAl₂O₄ on alumina surface. In order to prevent this change in nickel reducibility from impacting the catalyst performance, reduction prior to reactivity testing is performed at 700 °C, which is higher than the onset of nickel reduction for all samples (Figure 1a).

XRD patterns of calcined catalysts are collected to determine the phases in multi-component catalysts. XRD patterns of several calcined catalysts (Figure 1b) display primarily diffraction peaks corresponding to NiO. Only at the highest manganese loading investigated in this work (5Ni20Mn) do the diffraction peaks attributable to MnO₂ become visible. This corroborates with the hypothesis that the majority of manganese present on these multi-component catalysts is highly amorphous or in the form of very small particles. The intensity of the NiO diffraction peaks at the same Ni loading decreases with increasing manganese loadings, indicating that a mixed nickel-manganese oxide phase is likely formed rather than a physical mixture of NiO and MnO_x particles. However, this mixed oxide phase is likely amorphous, without any distinct diffraction pattern. This is consistent with the general amorphous nature of metal aluminates reported in the literature.^{42,44} Regardless of the presence or absence of mixed phases after calcination, the similar dispersions of all reduced catalysts (Table 1) strongly indicates that after reduction any Ni containing mixed oxides are reduced to the point that Ni is in a metallic state. Therefore, we do not expect any post-calcination mixed oxide phases to affect the reactivity or stability of our multi-component catalysts.

Table 1: Summary of synthesized catalysts (after reduction at 800 °C)

| Catalyst | Nominal Composition (Metals basis, balance γ -Al ₂ O ₃) | Actual Mn:Ni (Molar) (XRF) | Ni Dispersion (%) (CO Chemisorption) |
|----------|---|----------------------------|--------------------------------------|
| 5Ni | 5% Ni | - ^a | 3.28 ± ~0.12 |
| 5Ni2.5Mn | 5% Ni, 2.5% Mn | 0.56 ± ~0.03 | - ^a |
| 5Ni5Mn | 5% Ni, 5% Mn | - ^a | 3.69 ± ~0.12 |
| 5Ni7.5Mn | 5% Ni, 7.5% Mn | 1.41 ± 0.08 | - ^a |
| 5Ni10Mn | 5% Ni, 10% Mn | 1.99 ± 0.12 | 3.53 ± ~0.12 |
| 5Ni15Mn | 5% Ni, 15% Mn | 3.08 ± 0.18 | - ^a |
| 5Ni20Mn | 5% Ni, 20% Mn | 3.75 ± 0.22 | 3.55 ± ~0.12 |
| 10Mn | 10% Mn | - ^a | - ^a |
| NiB | 100% Ni | - ^a | - ^a |
| NiMnB | 33% Ni, 67% Mn | - ^a | - ^a |

^aNot determined.

Catalytic Evaluation with Model and Commercial Jet Fuel

In order to verify the proposed catalyst design strategy, a series of multi-component Ni-Mn catalysts are evaluated in steam reforming a model jet fuel stream. A tridecane feed with 300 ppm of sulfur in the form of 3-methylbenzothiophene is employed as a model stream. Tridecane is used as the model hydrocarbon for jet fuels because it has a similar average molecular weight and boiling point to jet fuels⁴⁵. In all reforming experiments a steam to carbon ratio of 3 is used. Figure 2a shows the time on stream (TOS) tridecane conversion in its steam reforming, as well as the product distribution, over 5Ni. The

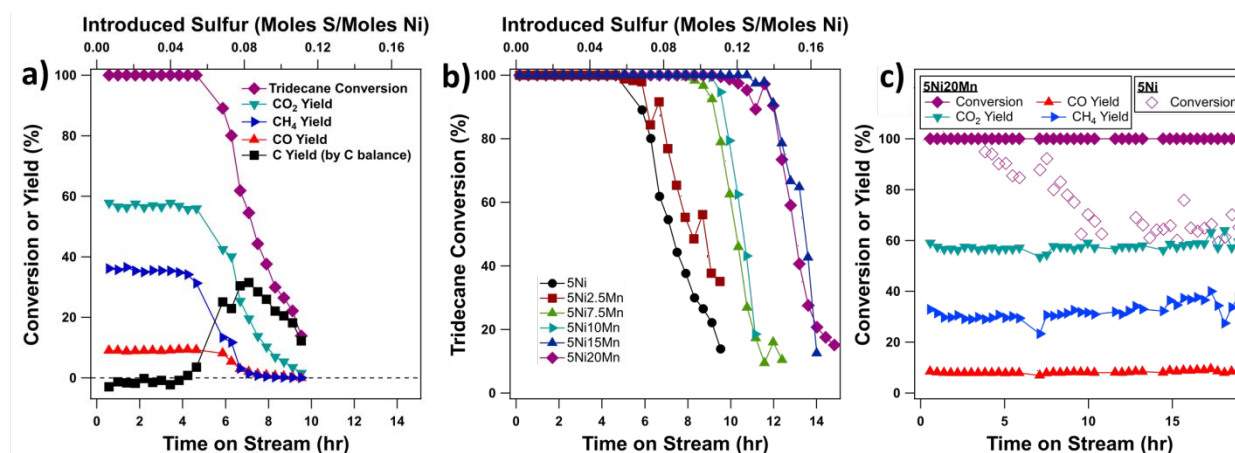


Figure 2: Catalyst evaluation in the reforming of 300 ppm S in tridecane at 500 °C and 130 mL g⁻¹hr⁻¹ of tridecane, and a steam to carbon ratio of 3 (a) reactivity 5Ni in reforming 300 ppm S in tridecane (b) comparisons of the catalyst deactivation for a range of coimpregnated Ni-Mn catalysts (c) Sulfur free reforming of tridecane over 5Ni and 5Ni20Mn. The top axes of (a) and (b) display the cumulative sulfur introduced to the catalyst in order to visualize sulfur capacity.

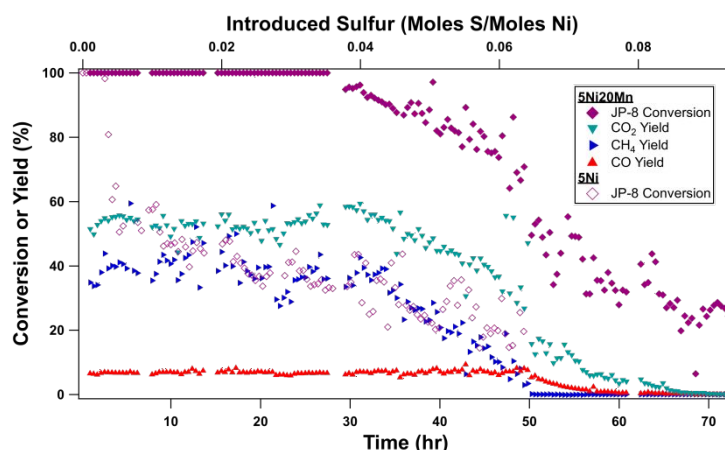


Figure 3: Catalyst evaluation in the steam reforming of JP-8 using 5Ni and 5Ni20Mn at 500 °C, 90 mL g⁻¹hr⁻¹ of JP-8, and a steam to carbon ratio of 3. The top axis displays the cumulative sulfur introduced to the catalyst in order to visualize sulfur capacity.

space velocity in the test (130 mL g⁻¹hr⁻¹ of tridecane) is chosen such that the initial tridecane conversion is complete and deactivation can be tracked over the course of several hours and is comparable to space velocities used in previous literature²⁵. Yields of CO, CO₂ and CH₄ roughly follow steam reforming equilibrium,⁴⁶ which is consistent with a previous report.²⁵ H₂ production is consistent with reforming stoichiometry (Figure S3). Significant catalyst deactivation is observed after roughly 5 h TOS, corresponding to the addition of roughly 0.06 mole of sulfur per mole of nickel in the catalyst bed. Figure 2b shows the TOS performance over multi-component Ni-Mn catalysts with varying amounts of co-impregnated manganese. A consistent trend of increasing catalyst stability with the Mn loading is observed, with the most sulfur resilient catalyst (5Ni20Mn) remaining active for roughly twice as long as the monometallic nickel catalyst. Both 5Ni and 5Ni20Mn are substantially more stable in sulfur free feeds (Figure 2c), though 5Ni does deactivate slightly while reforming sulfur free tridecane. Thus, the increased stability of the multi-component catalysts is a result of both sulfur resilience and resistance to coke formation. Similar resistance to coke formation has been observed in Ni-Mn multi-component catalysts during dry reforming^{47, 48} which Seok et al. attributed to the formation of surface carbonate species on MnO_x surfaces. While both deactivation route clearly occur on the monometallic Ni catalyst, sulfur deactivation is far more severe, resulting in nearly complete deactivation (<20% conversion) after 10 h TOS in the presence of sulfur (Figure 2.a) but remains partially active (~60% conversion) after 18 h TOS in sulfur free conditions (Figure 2.c). While we do not perform experiments in the kinetic regime to access the effect manganese addition has on the catalytic activity of our catalysts, it is well established in literature that Ni-Mn catalysts exhibit slightly higher rates in steam reforming than nickel catalysts^{35, 37}.

Enhanced S-resistance of the 5Ni20Mn catalyst as compared to that of the supported Ni catalyst is also observed in steam reforming of Jet Propellant 8 (JP-8), which is a widely used military jet fuel. JP-8 consists of a mixture of C₇-C₁₄ hydrocarbons, including linear, branched alkanes, alkenes and aromatics⁴⁹. The JP-8 sample employed in this study is determined by XRF to contain roughly 52 ppm of sulfur. In order to maintain the initial complete conversion of the fuel stream, a lower space velocity is used (90 mL g⁻¹hr⁻¹ of JP-8). The lower reactivity of JP-8 as compared to tridecane is likely due to

the presence of aromatics; which typically exhibit substantially slower kinetics in steam reforming on a per carbon basis than linear and cyclic hydrocarbons.⁵⁰ The time dependent conversion data for 5Ni catalyst compared to the most stable Ni-Mn catalyst (5Ni20Mn) during the steam reforming of JP-8 (Figure 3) demonstrates a dramatic difference in catalyst stability. 5Ni maintains complete conversion until roughly 0.003 moles of sulfur is fed per mole of Ni whereas the Ni-Mn catalyst maintains conversion until 0.035 moles of sulfur per mole Ni are introduced, i.e., more than one order of magnitude improvement. There is a notable difference in the sulfur capacity of the Ni-Mn catalyst between the model S-containing feed and JP-8. 5Ni20Mn maintains complete conversion until ~0.12 mole of sulfur per mole of Ni with the model feed but only ~0.04 mole sulfur per mole of nickel in JP-8. We tentatively attribute this difference to the increased heterogeneity of the hydrocarbon feed and the organosulfur species present with it in the case of JP-8. Methylbenzothiophene is employed as the sulfur source in tridecane as the model feed, however, JP-8 often contains several distinct types of organosulfur species including thiols, sulfides, disulfides, benzothiophenes, and dibenzothiophenes⁴⁹. While we generally expect all of these sulfur species to be relatively easily decomposed to H₂S in steam reforming conditions, substantial differences in the overall reactivity and catalyst sulfurization kinetics of various organosulfur species have been observed in the hydrodesulfurization literature^{51, 52}. Thus, we believe the difference in stability observed when using JP-8 as compared to our simplified model system is a result of select organosulfur species present in JP-8 contributing to catalyst deactivation more seriously than methylbenzothiophene does in the model feed stream employed in this work.

Post Reaction Catalyst Characterization

In order to elucidate the cause of the enhanced stability of the multi-component catalysts, spent catalysts have been characterized to understand carbon and sulfur deposition in this system. The measured S:Ni ratio of each spent catalyst is plotted against the measured Mn:Ni (Figure 4a and Table S2), which shows a clear upward trend. This is a strong indication that the introduction of Mn enhances the S tolerance of the catalyst with the identical Ni loading and similar density of surface Ni sites as determined by the CO

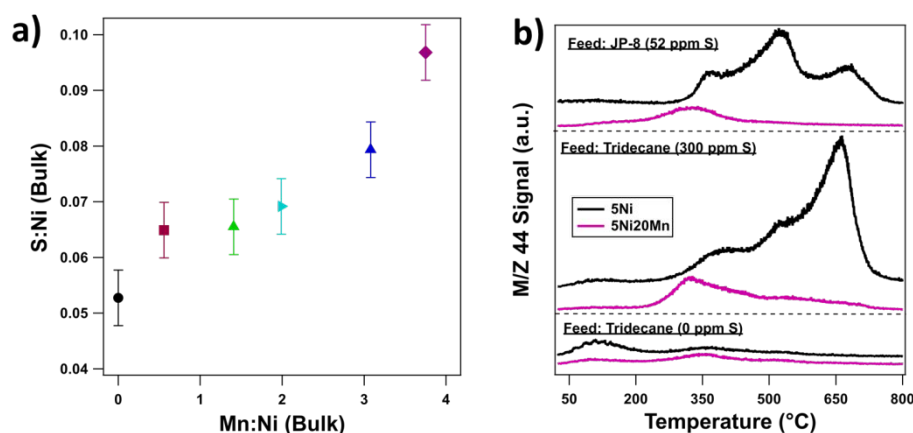


Figure 4: Characterization of carbon and sulfur deposits a) sulfur deposited on spent catalysts measured by XRF, and b) TPO signals for 5Ni and 5Ni20Mn after reaction in different feeds. TPOs are performed using a stream of 1% O₂ in He with a ramp rate of 10 °C/min with 20 mg of spent samples used in reactivity testing.

chemisorption. Further, the measured S:Ni ratio on the spent catalyst (Figure 4a) also increases with the TOS of the catalyst before the tridecane conversion begins to decrease from 100% (Figure 2b), indicating that the observed increase in the sulfur resistance is due to catalyst's enhanced capacity to adsorb sulfur without covering the active sites. This is consistent with our hypothesis that the introduction of a second strongly S-binding metal element could alleviate the S poisoning of Ni.

As our reactivity data shows both resistance to coke formation and sulfur poisoning, we also quantify and characterize carbon deposition on our spent catalysts via temperature programmed oxidation (TPO, Figure 4b). The 5Ni catalyst when subjected to both sulfur containing tridecane and JP-8 displays distinct oxidation peaks at several temperatures (~350 °C, ~520 °C, and ~670 °C) consistent with coke formation on nickel catalysts in reforming reactions⁵³. Meanwhile, the relative intensities of TPO peaks on the spent 5Ni catalyst operated in the S-containing tridecane and JP-8 are different, suggesting that the coke formation is sensitive to the identity of S-containing species in the feed. This hypothesis is further supported by the observation of much weaker TPO peaks on the spent 5Ni in the S-free tridecane, where the high temperature peak at ~670 °C is absent. Thus, S-containing species in the feed leads to the formation of surface sites that are prone to coking formation. By comparison carbon formation on the 5Ni20Mn catalyst is remarkably homogenous, possessing only one broad oxidation peak at ~350 °C regardless of feed composition or the inclusion of organosulfur species in the feed, indicating that the presence of Mn suppresses the formation of coke-inducing sites on the surface by the S-containing feed, and thus leading to different forms carbon deposition from those formed on nickel-based catalysts. In all cases the multi-component catalyst cokes significantly less than 5Ni.

Photoelectron spectroscopy (XPS) of spent catalysts confirms the formation of metal sulfides during reaction. XPS analysis is performed on spent unsupported samples, i.e., NiB and NiMnB, in order to increase the signal to noise ratio. XP spectrum of the spent NiB catalyst after reaction in a feed of tridecane contain 300 ppm

sulfur shows S_{2p3/2} and S_{2p1/2} peaks at 162.3 and 163.6 eV, respectively (Figure 5a), which are reasonably consistent with monolayers of sulfur on nickel in the literature⁵⁴. S_{2p} peaks at similar binding energies are observed on the spent NiMnB without any signals attributable to sulfate or sulfite. These observations indicate that in both cases only metal sulfides are formed. While the nickel and manganese phases in unsupported catalysts are similar to those of supported catalysts, XPS peak areas obtained on unsupported samples are unlikely to be quantitatively representative of that of the supported catalysts due to the different particle sizes and dispersions. Therefore, the lower intensity of the S_{2p} of the spent multi-component catalyst does not necessarily reflect its lower S content as compared to that of spent NiB. The S_{2p} peaks of spent NiMnB (full width at half max, FWHM = 3.3 eV) are substantially broader than those of the spent NiB (FWHM = 1.3 eV), indicating that bound sulfur on the spent multi-component catalyst is more chemically diverse. However, the similar binding energies of S_{2p} peaks among the most common Mn and Ni sulfides (within 1 eV)⁵⁴ make it difficult to determine the chemical nature of the metal sulfides formed during reaction.

Raman spectroscopy is also employed to elucidate the nature of the sulfur bound to the spent catalysts. To isolate the structural changes due to sulfur deactivation, Raman spectra of 5Ni and 5Ni20Mn catalysts are collected at 3 distinct stages: 1) after reduction with H₂ at 700 °C, 2) after reaction in a sulfur free feed of tridecane for 18 h, and 3) after reaction in a tridecane feed with 300 ppm sulfur in the form of 3-methylbenzothiophene until conversion drops significantly (Figure 2b). Nickel sulfide is known to have weak Raman signal and its precise assignment remains debated²⁹. In contrast, bulk manganese sulfide exhibits a strong Raman band at ~335 cm⁻¹ (Figure S4), and distinct Raman bands are present for MnS in the form of thin films⁵⁵. All three Raman spectra for 5Ni exhibit essentially the same features except for the evolution of graphitic and disordered carbon peaks at ~1580 cm⁻¹ and ~1380 cm⁻¹, respectively (Figure 5b). The representative low wave number band of NiAl₂O₄ is observed at ~600 cm⁻¹⁵⁶, as well as a secondary peak at ~1050 cm⁻¹, consistent with hydroxyl groups present in some nickel aluminate oxides⁵⁷. This is also consistent with the presence of the high temperature peak in

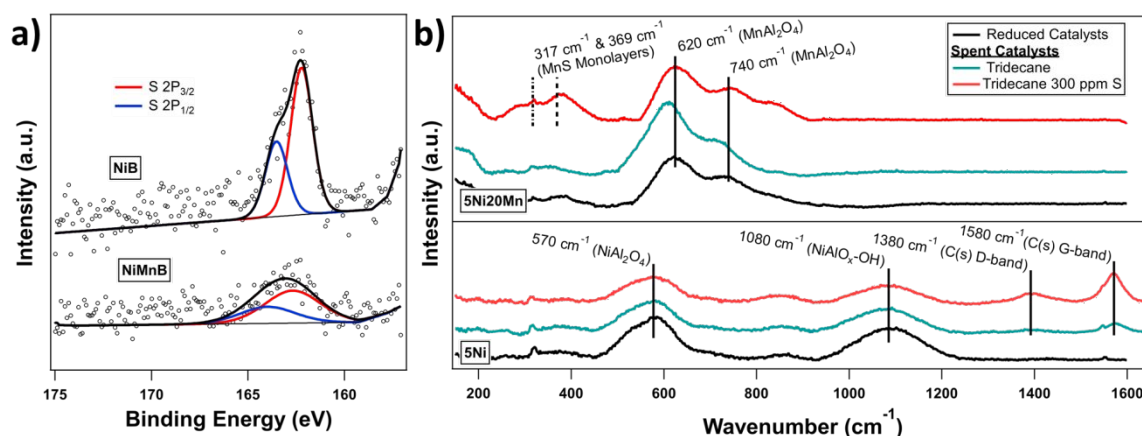


Figure 5: a) S_{2p} XPS spectra of spent NiB and NiMnB catalysts b) Raman spectra of spent 5Ni and 5Ni20Mn. Spent catalysts were subject to reforming conditions in either sulfur free tridecane (for 18 h) or tridecane with 300 ppm sulfur (until obvious deactivation, Figure 2b).

TPR profiles (Figure 1a). Similarly, the Raman spectra of 5Ni20Mn is essentially the same for the reduced catalyst and the spent catalyst exposed to a sulfur free tridecane feed (Figure 6b). The broad bands from ~ 450 to 800 cm^{-1} are consistent with the two most prominent Raman peaks of the $MnAl_2O_4$ spinel phase at ~ 640 , 700 , and 740 cm^{-1} ⁵⁸. The absence of the characteristic nickel aluminate peaks in the 5Ni20Mn further supports the hypothesis that the introduction of manganese disrupts the formation of $NiAl_2O_4$ in favor of $MnAl_2O_4$, increasing the reducibility of nickel significantly. The Raman spectra for the spent catalyst exposed to a sulfur containing stream shows a very broad peak from 230 to 460 cm^{-1} . This broad peak is roughly consistent with two broad peaks observed by Dhandayuthapani et al.⁵⁵ at 317 cm^{-1} and 369 cm^{-1} (dotted lines in Figure 5b). While this observed broad band is not as well defined as those observed by Dhandayuthapani et al., it could be attributed to fact that manganese sulfide or oxysulfide formed during the steam reforming is likely a disordered film on a relatively amorphous manganese oxide. The disordered structure is evidenced by the broadness of the peak. It is interesting to note that the 5Ni20Mn sample does not exhibit graphitic or disorder carbon bands after exposure to a sulfur containing feed despite forming a similar amount of carbon deposition to 5Ni exposed to sulfur free tridecane according to TPOs (Figure 4b). This observation together with the homogenous nature of the carbon deposit, as evidenced by the single peak in the TPO profile on the 5Ni20Mn catalyst (Figure 4b), leads us to conclude that carbon deposited on NiMn catalysts is primarily in the form of surface carbides or carbonates rather than graphitic or disordered carbon, as suggested by Seok et al.^{47, 48} This could play a role in the multi-component catalyst's ability to resist coke formation as compared to monometallic nickel catalysts.

Conclusions

In summary, we demonstrate that nickel-manganese catalysts possess substantially higher sulfur tolerance in the steam reforming of sulfur containing fuels than monometallic nickel catalysts due to a unique sulfur spillover effect from nickel particles to manganese oxide particles. This hypothesis is supported by means of detailed reactivity testing with both real

and model feeds and ex situ characterization of spent catalysts which indicate the formation of a poorly defined manganese sulfide or oxysulfide phase as a sacrificial sulfur adsorbent. While we cannot explicitly rule out other mechanisms by which this enhanced stability is achieved, the spectroscopic evidence of additional sulfide species alongside reactivity testing and post reaction sulfur measurements make this explanation quite likely. The deactivation behavior of the catalyst is clearly more complex when real jet fuel is used as a reforming feed. The multi-component catalyst is more stable than the monometallic nickel catalyst while reforming JP-8, however, all catalysts deactivate more quickly on a per sulfur basis while reforming JP-8 compared to methylbenzothiophene containing model feed.

Experimental

All catalysts are prepared using Ni (II) nitrate and Mn (II) nitrates (Sigma Aldrich) and dispersible boehmite (Dispal 23N4-80). After mixing, prepared impregnation gels are dried at $\sim 80\text{ }^\circ\text{C}$ overnight. Dried samples are calcined at $500\text{ }^\circ\text{C}$ for 6 hours under flowing air in a muffle furnace. All reactivity experiments are conducted in a fixed bed flow quartz tube microreactor. Gases are supplied by calibrated Brooks mass flow controllers and liquids (hydrocarbons and water) are supplied by two parallel Cole Parmer syringe pumps. All gas lines are maintained at least $230\text{ }^\circ\text{C}$ to prevent condensation of reactants and products. Gas analysis is performed using an online Agilent 7890A GC system with parallel channels for hydrocarbon quantification by FID and permanent gas quantification via TCD. All catalysts are prereduced at $700\text{ }^\circ\text{C}$ in a flow of pure H_2 before catalyst evaluation. JP-8 is a complex mixture of hydrocarbons which cannot be fully separated by GC (Figure S5); in order to calculate conversion, we assume all hydrocarbon species in JP-8 have similar response factors on a per carbon basis and treat JP-8 as a single reactant. XRDs are recorded using a Bruker D8 diffractometer with a Cu source. XRF is used to quantify bound sulfur and sulfur contents in JP-8 using a Rigaku Supermini 200 WDXRF. XPS spectra are collected using a Thermo Fisher K-Alpha+ system. TPRs and CO chemisorption experiments are

performed using a quartz tube microreactor system built in-house with a Gow-Mac TCD detector. TPRs are performed using a stream of 5% H₂ in N₂ at a flow rate of 50 mL/min with a ramp rate 5 °C/min to 800 °C following by a temperature hold until the TCD signal reaches a baseline. TPOs are performed using stream of 1% O₂ in He with a flow rate of 100 mL/min with a ramp rate of 10 °C/min to 800 °C using a Stanford Research Systems QMS100 to monitor CO₂ production via the m/z 44 signal. All flow reactors are controlled by integrated LabView programs developed in house. Raman spectra of spent catalysts are taken ex situ using a Horiba LabRAM system using a UV laser (325 nm).

Conflicts of interest

There are no conflicts to declare.

Acknowledgements

We acknowledge the support of US Air Force Office of Scientific Research (grant FA9550-18-1-0001) and appreciate the excellent characterization equipment maintained by the Advanced Materials Characterization Laboratory and the Surface Analysis Facility at UD.

Notes and references

- G. A. Whyatt and L. A. Chick, *Electrical generation for more-electric aircraft using solid oxide fuel cells*, Pacific Northwest National Lab.(PNNL), Richland, WA (United States), 2012.
- K. Rajashekar, J. Grieve and D. Daggett, 2006.
- J. E. Freeh, J. W. Pratt and J. Brouwer, 2004.
- J. E. Freeh, J. Steffen Jr and L. M. Larosiliere, 2005.
- D. F. Waters and C. P. Cadou, *J. Power Sources*, 2015, **284**, 588-605.
- V. Kharton, F. Marques and A. Atkinson, *Solid State Ionics*, 2004, **174**, 135-149.
- C. Duan, J. Tong, M. Shang, S. Nikodemski, M. Sanders, S. Ricote, A. Almansoori and R. O'Hayre, *Science*, 2015, **349**, 1321-1326.
- K.-D. Kreuer, *Ann. Rev. Mater. Res.*, 2003, **33**, 333-359.
- W. F. Taylor, 1997.
- J. G. McCarty, K. M. Sancier and H. Wise, *J. Catal.*, 1983, **82**, 92-97.
- J. G. McCarty and H. Wise, *J. Chem. Phys.*, 1982, **76**, 1162-1167.
- J. G. McCarty and H. Wise, *J. Chem. Phys.*, 1981, **74**, 5877-5880.
- J. G. McCarty and H. Wise, *J. Chem. Phys.*, 1980, **72**, 6332-6337.
- J. R. Rostrup-Nielsen, J. Sehested and J. K. Nørskov, 2002.
- J. Sehested, *Catalysis Today*, 2006, **111**, 103-110.
- J. G. McCarty and H. Wise, *J. Catal.*, 1985, **94**, 543-546.
- E. M. Fernández, P. G. Moses, A. Toftelund, H. A. Hansen, J. I. Martínez, F. Abild - Pedersen, J. Kleis, B. Hinnemann, J. Rossmeisl and T. Bligaard, *Angew. Chem. Int. Edit.*, 2008, **47**, 4683-4686.
- F. Abild-Pedersen, J. Greeley, F. Studt, J. Rossmeisl, T. Munter, P. G. Moses, E. Skulason, T. Bligaard and J. K. Nørskov, *Phys. Rev. Lett.*, 2007, **99**, 016105.
- R. A. Robie and B. S. Hemingway, *Thermodynamic properties of minerals and related substances at 298.15 K and 1 bar (105 Pascals) pressure and at higher temperatures*, US Government Printing Office, 1995.
- A. Zubkov, T. Fujino, N. Sato and K. Yamada, *J. Chem. Thermodyn.*, 1998, **30**, 571-581.
- E. G. Osadchii and O. A. Rappo, *Am. Mineral.*, 2004, **89**, 1405-1410.
- L. Cemič and O. Kleppa, *Phys. Chem. Miner.*, 1988, **16**, 172-179.
- J. A. Rard, *Chem. Rev.*, 1985, **85**, 1-39.
- K. Jacob and P. Gupta, *J. Chem. Thermodyn.*, 2014, **70**, 39-45.
- J. J. Strohm, J. Zheng and C. Song, *J. Catal.*, 2006, **238**, 309-320.
- S. L. Lakhapatri and M. A. Abraham, *Appl. Catal. A-Gen.*, 2009, **364**, 113-121.
- C. Xie, Y. Chen, Y. Li, X. Wang and C. Song, *Appl. Catal. A-Gen.*, 2010, **390**, 210-218.
- T. Kelly, G. Matos, C. DiFrancesco, K. Porter, C. Berry, M. Crane, T. Goonan and J. Sznopce, *Historical statistics for mineral and material commodities in the United States*, Report 2327-638X, US Geological Survey, 2005.
- Z. Cheng, H. Abernathy and M. Liu, *J. Phys. Chem. C.*, 2007, **111**, 17997-18000.
- M. Keller and R. Dieckmann, *Ber. Bunsenges. Phys. Chem.*, 1985, **89**, 883-893.
- J. L. Hudson, E. H. Johnson, D. F. Natusch and R. L. Solomon, *Environ. Sci. Technol.*, 1974, **8**, 238-243.
- S. Asaoka, H. Okamura, Y. Akita, K. Nakano, K. Nakamoto, K. Hino, T. Saito, S. Hayakawa, M. Katayama and Y. Inada, *Chem. Eng. J.*, 2014, **254**, 531-537.
- J. Wang, B. Liang and R. Parnas, *Fuel*, 2013, **107**, 539-546.
- D. H. Heo, R. Lee, J. H. Hwang and J. M. Sohn, *Catalysis Today*, 2016, **265**, 95-102.
- M. Koike, C. Ishikawa, D. Li, L. Wang, Y. Nakagawa and K. Tomishige, *Fuel*, 2013, **103**, 122-129.
- L. Dalin, Y. Nakagawa and K. Tomishige, *Chinese Journal of Catalysis*, 2012, **33**, 583-594.
- N. Hlaing, K. Kawahara, O. Nakagoe, G. Zheng, H. Sano and S. Tanabe, *Chem. Lett.*, 2018, **47**, 1131-1134.
- F. Morales, E. de Smit, F. M. de Groot, T. Visser and B. M. Weckhuysen, *Journal of Catalysis*, 2007, **246**, 91-99.
- F. M. Cano, O. Gijzeman, F. De Groot and B. Weckhuysen, in *Stud. Surf. Sci. Catal.*, Elsevier, 2004, vol. 147, pp. 271-276.
- J. Paterson, M. Peacock, R. Purves, R. Partington, K. Sullivan, G. Sunley and J. Wilson, *ChemCatChem*, 2018, **10**, 5154-5163.
- P. P. Nampi, S. Ghosh and K. G. Warriar, *Ceram. Int.*, 2011, **37**, 3329-3334.
- J. Zieliński, *J. Catal.*, 1982, **76**, 157-163.
- C. Li and Y.-W. Chen, *Thermochim. Acta*, 1995, **256**, 457-465.
- F. Kapteijn, A. D. Vanlangeveld, J. A. Moulijn, A. Andreini, M. A. Vuurman, A. M. Turek, J.-M. Jehng and I. E. Wachs, *J. Catal.*, 1994, **150**, 94-104.
- Permissible Exposure Levels for Selected Military Fuel*

- Vapors*, The National Academies Press, Washington, DC, 1996.
46. H. Zhu, B. L. Kee, C. Karakaya, R. O'Hayre and R. J. Kee, *Catal. Today*, 2017.
47. S.-H. Seok, S. H. Han and J. S. Lee, *Appl. Catal. A-Gen.*, 2001, **215**, 31-38.
48. S.-H. Seok, S. H. Choi, E. D. Park, S. H. Han and J. S. Lee, *J. Catal.*, 2002, **209**, 6-15.
49. K. D. F. Dietzel, University of Georgia, 2005.
50. J. R. Rostrup-Nielsen, *J. Catal.*, 1973, **31**, 173-199.
51. X. Ma, K. Sakanishi and I. Mochida, *Ind. Eng. Chem. Res.*, 1996, **35**, 2487-2494.
52. R. Shafi and G. J. Hutchings, *Catal. Today*, 2000, **59**, 423-442.
53. S. Natesakhawat, R. B. Watson, X. Wang and U. S. Ozkan, *Journal of Catalysis*, 2005, **234**, 496-508.
54. A. V. Naumkin, A. Kraut-Vass and C. J. Powell, *NIST X-ray photoelectron spectroscopy database*, Measurement Services Division of the National Institute of Standards and ..., 2008.
55. T. Dhandayuthapani, M. Girish, R. Sivakumar, C. Sanjeeviraja and R. Gopalakrishnan, *Appl. Surf. Sci.*, 2015, **353**, 449-458.
56. S. S. Chan and I. E. Wachs, *J. Catal.*, 1987, **103**.
57. J. Pérez-Ramirez, G. Mul and J. Moulijn, *Vib. Spectrosc.*, 2001, **27**, 75-88.
58. S. Zhai, Y. Yin, S. R. Shieh, Y.-Y. Chang, T. Xie and W. Xue, *Phys. Chem. Miner.*, 2017, **44**, 163-170.